

The SEASAT Radar Altimeter

J. L. MacArthur

A long-term goal of satellite altimetry, precision to within 10 cm, was achieved by SEASAT, which used several innovative techniques, including a micro-computer-based all-digital signal processor, to realize the desired performance. Before SEASAT failed, 1684 hours of high-quality altimetry data were collected that will contribute to improved marine geoid modeling and to refined techniques for extracting information on oceanic processes.

Introduction

The concept of orbiting a precision altitude-measuring instrument goes back to the late 1960's. Prior to that time, beginning with Sputnik I in 1957, doppler tracking of satellites had resulted in the determination of a global geoid to resolve structure down to a scale of about 15° , or 1500 km. The geoid may be conceptualized as the equipotential surface of the earth's gravity field to which the waters of the sea would conform if all external forces were removed and the surface were to become still. The form of the geoid closely approximates an ellipsoid of revolution, with an equatorial radius of 6378.1 km and a polar radius about 21.4 km less. Deviations in the geoid from this "reference ellipsoid" can approach 100 m, most of which is accounted for in the satellite-derived geoid models. However, within a 15° square there can be variations of as much as 15 m. Where local surface-gravity data are available, even these variations can be largely accounted for. However, acquisition of such data from surface ships is a costly and time-consuming process. A strong argument could thus be made for orbiting an altimeter to provide synoptic measurements of sea surface topography from which fine grain undulations in the mean sea level, and hence the geoid, could be derived.¹

A height measurement precision of one or two meters would be important to geodesy. At the same time, it was recognized that somewhat better precision was required to attract the attention of the oceanographer and meteorologist interested in sea surface deviations from the geoid that result from currents, tides, atmospheric pressure, and standing winds. Variations of one meter and less could be expected from these influences and, accordingly, a long-term goal of 10 cm rms altimetry was stated.² It should be recognized that below a precision of about one meter rms, the topographic signal will contain a mixture of geoid, orbit, and ocean dynamics effects, the sorting out of which poses a major data analysis task.

Altimeter Evolution

Three satellite altimeters have been flown under NASA sponsorship. The first was on SKYLAB in 1973, the second on GEOS-3 (launched in March 1975), and the latest on SEASAT. All three altimeters are basically conventional, monostatic, pulsed radars that track in range only. Their design features are compared in Table 1. Sequential improvements in height measurement precision have resulted primarily from narrower pulse resolutions, although in the case of SEASAT an increase in

¹ G. C. Weiffenbach, "The GEOS-C Radar Altimeter," presented at Marine Technology Society 2nd Symposium on Marine Geodesy, Nov. 3-5, 1969.

² W. M. Kaula, *The Terrestrial Environment: Solid Earth and Ocean Physics*, NASA CR-1579 (1969).

Table 1

A COMPARISON OF ALTIMETER PARAMETERS

| | SKYLAB | GEOS-C (intensive) | SEASAT |
|------------------------------|--------|-----------------------|-------------|
| Mean altitude (km) | 435 | 840 | 800 |
| Antenna beamwidth (deg) | 1.5 | 2.6 | 1.6 |
| Frequency (GHz) | 13.9 | 13.9 | 13.5 |
| Peak RF power (kW) | 2 | 2 | 2 |
| Average RF power (W) | 0.05 | 0.24 | 6.5 |
| Pulse width (uncompressed) | 100 ns | 1 μ s | 3.2 μ s |
| Pulse width (compressed, ns) | — | 12.5 | 3.125 |
| Repetition frequency (Hz) | 250 | 100 | 1020 |
| Footprint diameter (km) | 8 | 3.6 | 1.7 |
| Altitude precision (rms) | <1 m | <50 cm | <10 cm |

pulse rate to 1020 Hz also contributed to a reduction in tracking noise.

The objective of the SKYLAB altimeter experiment was to demonstrate the concept and to acquire information needed in designing future precision altimeters.³ Thus the design of the instrument flown on GEOS-3, a dedicated altimetry satellite, was accomplished with every expectation of success. Indeed, in over three years of operation, data from GEOS-3 have led to many advances in using and interpreting altimeter data. In addition to the basic height measurement that provides information on oceanic processes and on the marine geoid, data on signal strength provide a measure of surface reflectivity from which, among other things, the boundaries of sea ice are revealed and wind speed may be inferred. Also, resolution of the signal returned from the ocean surface into a series of contiguous range samples allows significant waveheight (four times the rms wave height) to be determined and, in conjunction with the windspeed measurement, has the potential for distinguishing wind-driven waves from swell. Waveform shape analysis has also been shown recently to provide an indication of dominant wavelength.⁴

The improved resolution and precision of the SEASAT altimeter will extend the useful range of the data over and above what has been accomplished with GEOS-3. Of equal importance, however, was the inclusion on SEASAT of on-board

tape-recorder data storage to provide continuous data coverage on the earth's surface along the subsatellite track. Prior to the untimely failure of the SEASAT spacecraft after only 99 days of operation, some 1684 hours of high-quality altimetry data were collected. By comparison, this represents about 90% of the operating hours accumulated by GEOS-3 (which had no on-board recorder) during 3½ years of real-time operation. Analysis of the SEASAT data is proceeding. It is reasonable to anticipate further advances in altimetry applications and new requirements for the next generation instrument design.

Signal Characteristics

A discussion of the properties of the radar signal reflected from the ocean surface explains some of the design choices reflected in the SEASAT altimeter. Referring to Fig. 1, a pulse of energy radiates from the antenna in an expanding spherical wavefront whose intersection with the surface defines an instantaneous illuminated area, or "footprint." The concentric rings denote successive locations of an expanding annulus whose boundaries are the loci of points equidistant to the satellite, separated by the basic radar resolution, Δr , which is defined as

$$\Delta r = \frac{c\tau}{2}, \quad (1)$$

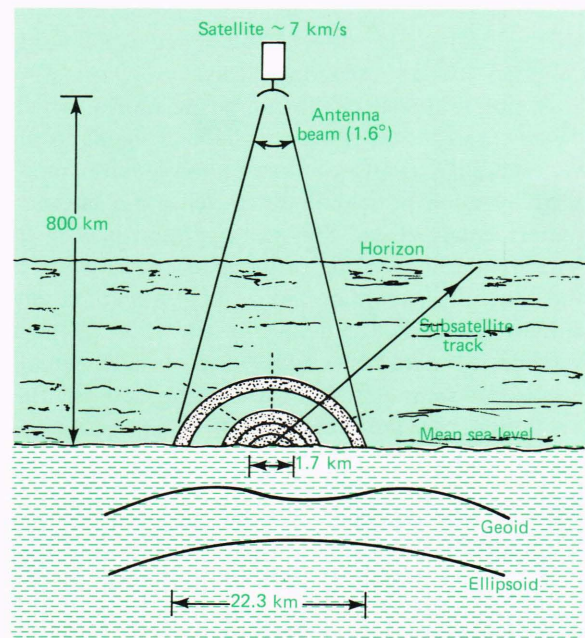


Fig. 1—Satellite altimeter geometry.

³ J. T. McGoogan, L. S. Miller, G. S. Brown, and G. S. Hayne, "The S-193 Radar Altimeter Experiment," *Proc. IEEE* No. 6, pp. 793-803 (1974).

⁴ E. J. Walsh, *Analysis of GEOS-3 Altimeter Data and Extraction of Ocean Waveheight and Dominant Wavelength*, NASA TM-73281 (1979).

where

Δr is the range resolution in meters,
 c is the speed of light (3×10^8 m/s), and
 τ is the radar pulse width (3.125 ns for
 SEASAT).

Because each reflecting point, or facet, on the surface returns a replica of the transmitted pulse (much reduced in amplitude), the boundaries represent areas within which reflected signals overlap in time and thus add together to contribute to the total signal contained within a resolution element of width Δr . For SEASAT, about 166 range cells were contained within the overall illuminated area defined by the 1.6° antenna beamwidth. The general condition in which the pulse resolution defines a region or regions within the overall antenna pattern is called the “pulse-width-limited” geometry.

A small-angle, flat-earth approximation results in an equal area for each concentric ring. For all but the calmest waters, each area contains many facets normal to the line-of-sight that contribute to the total signal. The equal area condition implies equal power returned per ring, and the presence of many contributing reflections within a range resolution element gives rise to noise-like amplitude statistics for the composite signal. The average signal has the form of a step function with an equal return from the nadir cell and succeeding cell. The signal rise time for calm seas is limited by the pulse width but, for waveheights above a meter or so, the leading edge slope is dominated by the vertical distribution of reflecting facets.

A simple model of the composite return, which closely matches the observed shape of signal power versus time, is a gaussian distribution function modified by an exponential decay reflecting antenna pattern attenuation. This is illustrated in Fig. 2. The standard deviation of the gaussian function is the root-sum-square of radar pulse spreading and rms waveheight. Processing to extract height and waveheight data will make use of gate signals formed by summing contiguous samples at the full resolution, as is described below.

Signal Processing

In common with many high-resolution pulsed radars, the altimeter uses a pulse compression technique to satisfy jointly the need for a wide bandwidth (for resolution) and high pulse energy (for detection). The transmitted frequency sweeps over

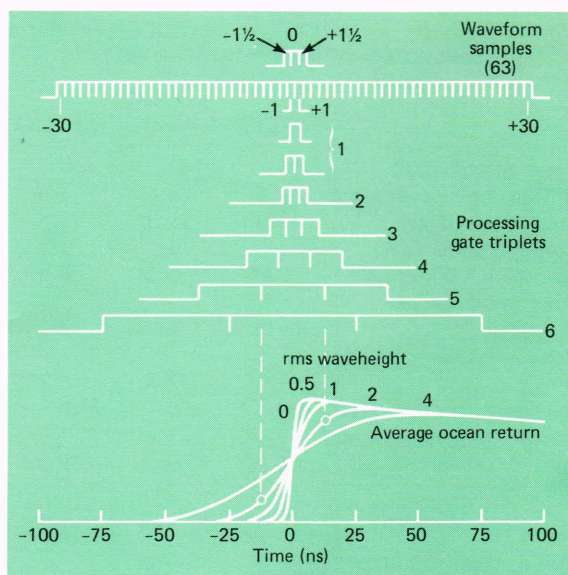


Fig. 2—Average ocean return signal and the formation of processing gates.

a 320 MHz band during each $3.2 \mu\text{s}$ pulse to allow a 3.125 ns compressed pulse width along with a 312.5 kHz noise bandwidth in the receiver. For the 2 kW transmitter power, the effect is like that of using a 2 MW pulse of 3.125 ns width. The linear FM (“chirped”) pulse also allows the use of an unusual method of received signal processing known as “full-deramp”.

This concept is illustrated in Fig. 3. Signals reflected from the ocean surface are mixed with a local oscillator that is itself a chirped pulse, rather than the usual continuous wave signal. The result is that the arrival time of a signal returned from a particular facet on the surface is transformed into the signal frequency after the first mixing operation. In other words, the system cannot distinguish between slight offsets of time and frequency. We can

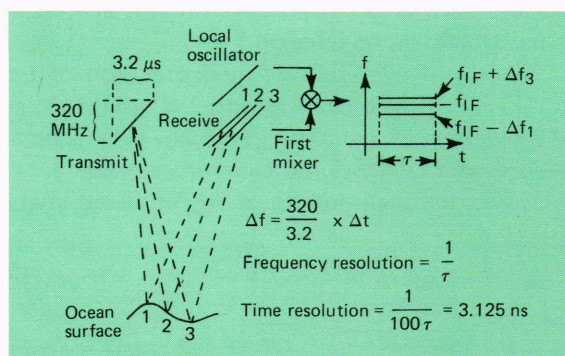


Fig. 3—Full-deramp processing.

take advantage of this by sorting signals according to frequency at the mixer output to determine their range with respect to the local-oscillator pulse. The frequency slope of the transmitted pulse is 100 MHz/ μ s; thus two facets separated by 3:125 ns in range would transform into pulses separated by 312.5 kHz. This is also the bandwidth of a filter matched to the 3.2 μ s pulse envelope; thus a bank of such filters can provide the contiguous range samples shown in Fig. 2. These samples provide the basic signal waveform data that are used to close a height-tracking loop and to estimate waveheight. The total filter bank is confined to a band of less than ± 10 MHz even though the transmitted pulse has a 320 MHz bandwidth. The bandwidth compression afforded by the full-deramp processing makes it possible to form the filter bank digitally using readily available medium-speed devices, which in turn minimize the complexity and power consumption of the altimeter.

The essential features of the complete instrument are shown in Fig. 4. Under control of a closed loop tracker, the chirped local-oscillator pulse is timed to bracket the received signals of interest. Because they are spread ± 100 ns about the track point, signals at the outer extremes of the range coverage experience a negligible truncation loss. All received signal information is confined to the 3.2 μ s local-oscillator pulse interval and is captured first by mixing to baseband in order to generate in-phase (I) and quadrature (Q) bipolar video signals. Then 64 samples of I and Q video signals at 50 ns steps are converted to 5-bit digital words and stored for subsequent processing in the interpulse period. Finally, filters that correspond to range samples are formed sequentially using the same hardware by repetitively accessing the 64 stored samples and implementing the equivalent of a dis-

crete Fourier transform in conjunction with a sine/cosine look-up table in read-only memory (ROM). As each filter is formed, the ROM addresses increment or decrement in uniform steps of phase, with a step size set by the center frequency of the filter. This in turn is set by the location within the overall filter bank along with an offset common to all filters, representing fine range.

Centering the ocean return within the filter bank thus involves coarse timing of the local-oscillator pulse in 12.5 ns steps and fine positioning of the filter bank (range samples) over a ± 625 kHz (± 6.25 ns) range. The finest step in range is 0.05 ns, or a frequency step of 5 kHz. This granularity would be difficult to achieve with more conventional time-domain processing.

Adaptive Tracker

Information contained in the waveform samples represented by the filter bank outputs is processed in an adaptive tracker to yield a estimate of significant waveheight based on leading-edge rise time; this, in turn, is used to adjust height-tracking loop parameters to compensate for the effect on tracker bandwidth and damping of waveheight variation up to 20 m.

The adaptive tracker is a microcomputer built around an 8080 microprocessor (Fig. 5).⁵ The read-only program-storage memory consists of 4096 8-bit bytes and the read-write storage memory consists of 2048 8-bit bytes. Dual buffers alternately accumulate waveform sample data for 50 pulse returns and hold the data for processing. Height tracking, automatic gain control (AGC),

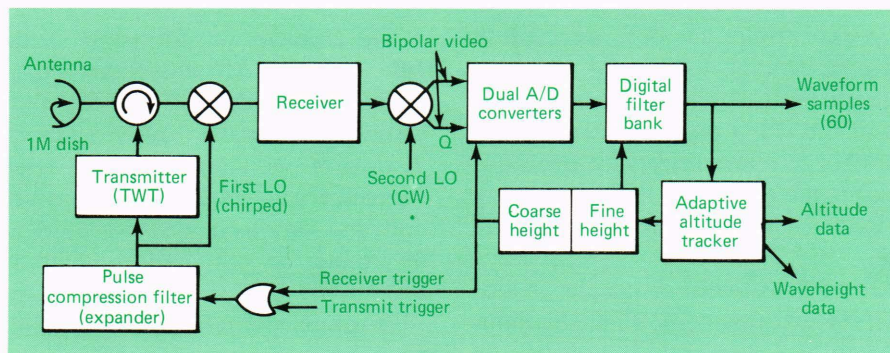


Fig. 4—Simplified block diagram of the altimeter.

⁵ J. A. Perschy, "The SEASAT-A Satellite Radar Altimeter Spaceborne Microcomputer," *J. Br. Interplanet. Soc.* **32**, No. 1, pp. 9-14 (1979).

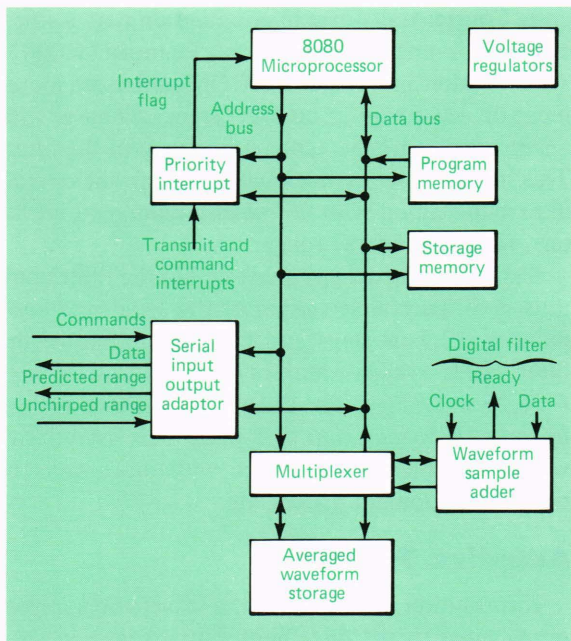


Fig. 5—Block diagram of the adaptive tracker.

and waveheight estimation algorithms are then implemented at a rate of 20 per second based on the smoothed waveform samples. The adaptive tracker also decodes commands to sequence the altimeter through acquisition, track, and calibration states and formats science and engineering data for telemetry. Telemetry output consists of 85 10-bit words at a rate of 10 per second. These include height, height error, height rate, AGC waveform samples, waveheight, commutated engineering data, and mode/status words.

Adaptive processing begins with the formation of a set of gate triplets by averaging groups of contiguous waveform samples to form gates of progressively increasing width, as suggested by Fig. 2. The early and late gate signals enter into waveheight estimation; the middle gate is used in height tracking once a gate triplet has been selected. A late-early difference signal is formed for each gate pair and the result most closely corresponding to samples taken at the $\pm 1 \sigma$ points on the leading edge of the normalized return selects the operative triplet. A look-up table derived from the ocean return model is then entered to derive the waveheight estimate.

An average of all 60 waveform samples is also formed that serves two functions. First, by comparing the average to a fixed reference value, an error signal is derived for use in closing an AGC

loop via a digital attenuator in the receiver. Properly calibrated, the AGC value is a measure of the ocean-surface reflectivity coefficient. Second, with scaling to account for the exponential decay caused by the antenna pattern, the 60 sample average provides a reference level equal to the leading edge "half-power" point where the signals intersect at all waveheights. By comparing this reference level to the amplitude of the previously selected middle gate, an error signal is derived for use in closing the height tracking loop. By adjusting receive timing via a closed-loop α, β tracker, the error signal is driven to zero on the average with the middle gate aligned to the midpoint of the ocean return's leading edge.

The form of α, β tracker used in the altimeter can be explained in terms of the following recursion equations, which result in smoothed estimates of height (h) and height rate (\dot{h}) based on the height error (Δh) measured as described above:

$$\dot{h}_n = \dot{h}_{n-1} + \frac{\beta}{T} \Delta h_{n-1}, \text{ and} \quad (2)$$

$$h_{n+1} = h_n + \alpha \Delta h_{n-1} + \dot{h}_n T. \quad (3)$$

Waveform samples are averaged for 50 pulse returns ($T = 49$ ms) prior to the formation of gates and the generation of a height error. Computation of updated quantities then takes place in the following 49 ms interval, after which the new values are applied to position the waveform samples. This process adds a 49 ms delay in the loop that will have an effect on dynamic behavior. Choice of the scaling constants α, β establishes the closed-loop bandwidth and damping. Selected values for the primary tracking mode are $\alpha, \beta = 1/4, 1/64$, which sets the loop time constant at 0.2 s.

On-Orbit Performance Results

The altimeter was turned on for the first time on July 3, 1978. All indications were that the performance was normal, and the altimeter was declared operational on July 7, 1978. During the next 30 days of operation, a detailed assessment of performance was conducted. The altimeter was operated in various modes to acquire a set of data to determine the optimum configuration for future operations.

Of primary interest is the height measurement precision, or noise. Figure 6 compares noise data taken during two consecutive orbits on July 10,

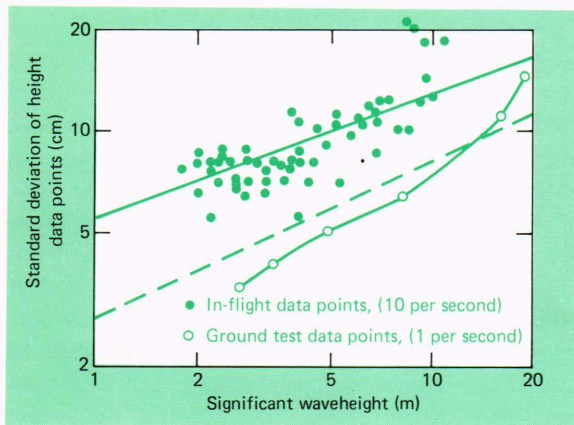


Fig. 6—Comparison of the precision of height measurement in flight with ground test data. A linear fit to the in-flight data (solid line) has been adjusted to reflect 1-s averaging (dashed line) for comparison with the test data.

1978 (when waveheights between 2 and 11 m were observed) with prelaunch test data. The standard deviation of in-flight height data points about a linear fit to 46 telemetry readouts at the rate of 10 readouts per second are plotted versus significant waveheight. To permit comparison with ground test data representing 1 s averages (10 telemetry data points), a linear fit to the in-flight data (solid line) has been adjusted to correspond to 1 s averaging (dashed line). The scaling used to do this was based on observed differences during ground test and is related to the height-tracking filter time constant. When compared on this basis, the in-flight and ground test data correlate quite well

and serve to demonstrate a 10-cm measurement precision for waveheights below about 15 m. At very low waveheights the precision approaches 3 cm.⁶

The stability of the height measurement over time is important because even slow drift in the altimeter readout can appear as an error in the geoidal component of height. To correct for this, the altimeter incorporated a built-in calibration mode in which a sample of the transmitted pulse was applied to the receiver and tracked as a point return to reveal long-term drift in the height data. A maximum drift rate of 50 cm/h and an ability to correct the height data to within ± 25 cm were specified. In-flight data have shown that the drift is small enough so as not to require corrections in order to comply with the requirement. Calibration-mode height bias measured just after launch agreed closely with that measured during ground testing at APL. Data taken just before the failure of SEASAT showed a drift of only -1.5 cm over an 85 day period. While this correction, as well as that for calibration mode data taken throughout the mission, can be applied to the height data for the ultimate in accuracy, the altimeter bias and drift were well within the specified requirement.

Verification of the altimeter's waveheight measurement capability took place during the Gulf of Alaska SEASAT Experiment (GOASEX) con-

⁶ SEASAT-1 Radar Altimeter Phase I Engineering Assessment Report, NASA TM-73279 (1978).

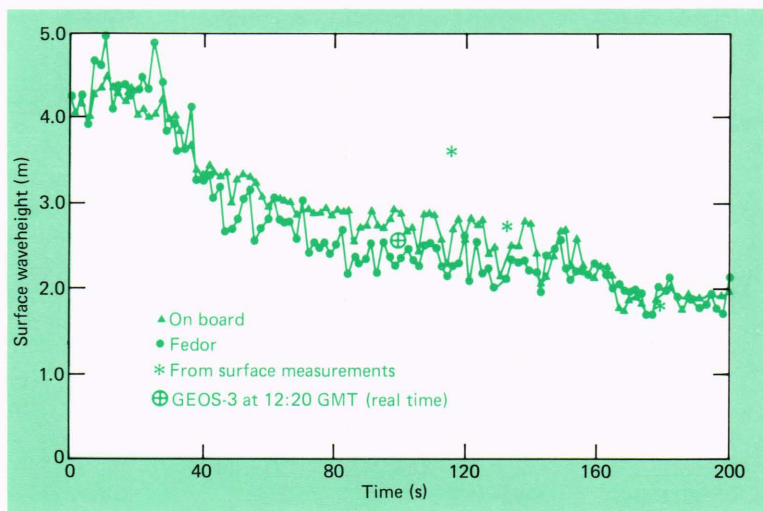


Fig. 7—Surface waveheights from on-board altimeter measurements and Fedor's ground processing algorithm.

ducted in September 1978.⁷ A variety of surface truth measurements was made during this exercise to evaluate the data from all SEASAT instruments. Surface ships, buoys, aircraft underflights, and one GEOS-3 pass were used. An example of the waveheight data is given in Fig. 7. A comparison of the on-board altimeter measurement with that of a somewhat more sophisticated ground processing algorithm (Fedor's) is also shown. The points asterisked were taken from a contour chart derived from surface measurements by the Navy's

Fleet Numeric Weather Center for 1200Z on September 16, 1978, the date of the pass. Correlation of satellite data with surface measurements made at slightly different times and locations can result in occasional discrepancies because of the changing nature of the ocean processes. Nevertheless, 68% of all waveheight comparisons (of which this figure is a small sample) differed by less than 0.5 m from the surface truth value for waveheights up to 4 m (the highest observed during GOASEX). This corresponds to the accuracy requirement allotted to the instrument alone. The single GEOS-3 data point provided further corroboration of the accuracy of the altimeter waveheight measurement.

⁷SEASAT Gulf of Alaska Workshop Report (Draft), Jet Propulsion Laboratory Document 622-101 (1979).

PUBLICATIONS

Principle books and technical articles published by APL staff members
July 1977 – December 1978

- L. C. Aamodt and J. C. Murphy, "Size Considerations in the Design of Cells for Photoacoustic Spectroscopy. II. Pulsed Excitation Response," *J. Appl. Phys.* **49**, No. 6, 1978, pp. 3036–3045.
- R. C. Adams (APL) and J. M. Cohen (Univ. Pennsylvania), "Analytic Supernova Models and Black Holes," *Int. J. Theoret. Phys.* **16**, No. 1, 1977, pp. 35–52.
- F. J. Adrian, "Radical Pair Mechanism of Chemically Induced Magnetic Polarization," *Chemically Induced Magnetic Polarization*, D. Reidel, Dordrecht-Holland, 1977, pp. 77–105.
- F. J. Adrian, "Triplet Overhauser Mechanism of CIDNP," *Chemically Induced Magnetic Polarization*, D. Reidel, Dordrecht-Holland, 1977, pp. 369–381.
- F. J. Adrian and A. N. Jette, "Valence Bond Study of Hyperfine Interactions and Structure of the Noble Gas Monohalides," *J. Chem. Phys.* **68**, No. 10, 1978, pp. 4696–4706.
- T. P. Armstrong and G. Chen (Univ. Kansas), E. T. Sarris (Max-Planck Inst. für Aeronomie), and S. M. Krimigis (APL), "Acceleration and Modulation of Electrons and Ions by Propagating Interplanetary Shocks," *Study of Travelling Interplanetary Phenomena*, D. Reidel, Dordrecht-Holland, 1977, pp. 367–389.
- T. P. Armstrong (Univ. Kansas), S. M. Krimigis (APL), and R. P. Leping (NASA/Goddard), "Magnetosheath Bursts of Predominantly Medium Nuclei Observed with Imp 8 on February 16, 1974," *J. Geophys. Res.* **83**, No. A11, 1978, pp. 5198–5206.
- A. Arrow and D. J. Yost, "Large Angle-of-Attack Missile Control Concepts for Aerodynamically Controlled Missiles," *J. Spacecr. Rockets* **14**, No. 10, 1977, pp. 606–613.
- W. H. Avery, "Ocean Thermal Energy—Status and Prospects," *Mar. Technol. Soc. J.* **12**, No. 2, 1978, pp. 9–16.
- C. B. Barger and R. B. Givens, "Localized Corrosion of Aluminum: Blister Formation as a Precursor of Pitting," *J. Electrochem. Soc.* **124**, No. 12, 1977, pp. 1845–1848.
- C. B. Barger and R. B. Givens, "Source of Oscillations in the Anode Current during the Potentiostatic Pitting of Aluminum," *J. Electrochem. Soc.* **124**, No. 8, 1977, pp. 1230–1232.
- R. J. Bartlett (Battelle) and S. Wilson and D. M. Silver (APL), "Third-Order Many-Body Perturbation Theory for the Ground State of the Carbon Monoxide Molecule," *Int. J. Quantum Chem.* **XII**, 1977, pp. 737–757.
- R. C. Benson and H. A. Kues, "Absorption and Fluorescence Properties of Cyanine Dyes," *J. Chem. Eng. Data* **22**, No. 4, 1977, pp. 379–383.
- R. C. Benson and H. A. Kues, "Fluorescence Properties of Indocyanine Green as Related to Angiography," *Phys. Med. Biol.* **23**, No. 1, 1978, pp. 159–163.
- J. F. Bird, "Hydromagnetism Induced by Submerged Acoustic Sources: Sonomagnetic Pseudoradiation," *J. Acoust. Soc. Am.* **62**, No. 5, 1977, pp. 1291–1296.
- J. F. Bird (APL) and R. W. Massof (JHMI), "A General Zone Theory of Color and Brightness Vision. II. The Space-Time Field," *J. Opt. Soc. Am.* **68**, No. 11, 1978, pp. 1471–1481.
- H. D. Black, "An Easily Implemented Algorithm for the Tropospheric Range Correction," *J. Geophys.*